Aerosol Science and Technology
Publication details, including instructions for authors and subscription information:
http://www.informaworld.com/smpp/title~content=t713656376

On Measuring the Critical Diameter of Cloud Condensation Nuclei Using Mobility Selected Aerosol

Markus D. Petters [a]; Anthony J. Prenni [a]; Sonia M. Kreidenweis [a]; Paul J. DeMott [a]
[a] Department of Atmospheric Science, Colorado State University, Fort Collins, Colorado, USA

First Published on: 01 October 2007

To cite this Article Petters, Markus D., Prenni, Anthony J., Kreidenweis, Sonia M. and DeMott, Paul J.(2007)'On Measuring the Critical Diameter of Cloud Condensation Nuclei Using Mobility Selected Aerosol',Aerosol Science and Technology,41:10,907 — 913
To link to this Article: DOI: 10.1080/02786820701557214
URL: http://dx.doi.org/10.1080/02786820701557214

Aerosol Science and Technology, 41:907–913, 2007

ISSN: 0278-6826 print / 1521-7388 online
DOI: 10.1080/02786820701557214

On Measuring the Critical Diameter of Cloud Condensation Nuclei Using Mobility Selected Aerosol

Markus D. Petters, Anthony J. Prenni, Sonia M. Kreidenweis, and Paul J. DeMott
Department of Atmospheric Science, Colorado State University, Fort Collins, Colorado, USA

Cloud condensation nuclei (CCN) instruments determine the so-called "critical diameter" for activation of particles into cloud droplets at a fixed water supersaturation. A differential mobility analyzer is often used to size-select particles for purposes of scanning for the critical diameter. Usually the diameter where 50% of the particles have activated to cloud droplets is assumed to be equal to the critical diameter. We introduce a model that describes the transfer of polydisperse charge-equilibrated particles through an ideal differential mobility analyzer followed by transit through an ideal CCN instrument. We show that if the mode diameter of the polydisperse size distribution exceeds the critical diameter of the particles, multiply-charged particles may lead to nonmonotonic CCN counter response curves (plots of CCN-active fraction vs. mobility diameter) that exhibit multiple peaks, rather than a simple sigmoidally-shaped curve. Hence, determination of the 50% activation diameter is ambiguous. Multiply-charged particles significantly skew the CCNc response curves when sampling particles with critical diameters exceeding 0.1 μm from particle size distributions with mode diameters also larger than the critical diameter. We present a method for inversion of CCN counter data that takes multiple-charging effects into account, and demonstrate its application to laboratory data. Our calculated CCN counter response curves are in good agreement with observations, and can be used to infer the critical activation diameter for a specified supersaturation.

Received 12 July 2006; accepted 5 July 2007.

We thank Paul J. Ziemann, Yong B. Lim, and Aiko Matsunaga for the aerosol generation and SMPS size distribution measurement. We also thank Jefferson R. Snider for reviewing an early draft of this manuscript. This research was supported by the U.S. National Science Foundation under grant ATM-0436196. Partial support was supplied by the Office of Science (BER), U.S. Department of Energy, under DE-FG02-05ER63984 and the National Aeronautics and Space Administration, under NNG04GR44G. We thank two anonymous reviewers for helpful comments. In particular we thank the reviewer who alerted us to the possibility that standard inversion techniques could be applied with no further modifications to also retrieve the activation diameter. We also thank Ulrike Dusek for calculating the activation diameters for our data based on the Frank et al. (2006) model. Finally we thank Rick Flagan for useful discussions about this manuscript. Any opinions, findings, and conclusions or recommendations expressed in this material are those of the authors and do not necessarily reflect the views of the National Science Foundation.

Address correspondence to Markus D. Petters, Department of Atmospheric Science, Colorado State University, Fort Collins CO, 80525-1371, USA. E-mail: petters@atmos.colostate.edu

1. INTRODUCTION

Large uncertainties about the effect of carbonaceous and other types of particles on cloud microphysical properties have spawned intensive research on their ability to act as cloud condensation nuclei (CCN). For example, several research groups have measured the critical diameter that must be exceeded before organic particles can serve as CCN when exposed to a fixed supersaturation inside a CCN instrument (e.g., Cruz and Pandis 1997; Corrigan and Novakov 1999; Prenni et al. 2001; Shantz et al. 2003; Bilde and Svenningsson 2004; Broekhuizen et al. 2004a). In these activation experiments, polydisperse aerosol is charge equilibrated and made quasi-monodisperse in a differential mobility analyzer (DMA). Then the flow containing the quasi-monodisperse particle distribution is split, with equal concentrations being sent to a CCN counter sampling at fixed supersaturation and a to condensation particle counter (CPC). For each mobility-selected size, the ratio of CCN to CPC concentration defines the so-called CCN active fraction. The diameter where 50% of the particles are CCN active (D_{50}) is generally interpreted as the critical dry diameter. Sometimes the critical diameter is defined as the *wet* critical diameter, i.e., the equilibrium diameter at the critical supersaturation. Here we define the critical diameter as the minimum *dry* diameter required for CCN activation at a specified supersaturation. Although most studies recognize the presence of multiply-charged particles, they do not quantitatively account for their contribution in determining D_{50} (Roberts and Nenes 2005; Dinar et al. 2006).

We introduce a model that describes the transfer of polydisperse charge-equilibrated particles through an ideal DMA, followed by transit through an ideal CCN counter (CCNc). If the particles are internally mixed, have identical composition and surface tension is not a function of particle size, then Köhler theory predicts that all particles larger than D_c activate if the environmental supersaturation is held constant. In this work, we assume this idealized behavior for a quasi-monodisperse population, size selected for a single mobility diameter using a DMA. We also account for the presence of larger, multiply-charged particles when calculating the CCN active fraction. Repeating the calculation for several mobility-selected diameters produces the calculated CCNc response curve. Using these model calculations we demonstrate that multiply-charged particles may lead to

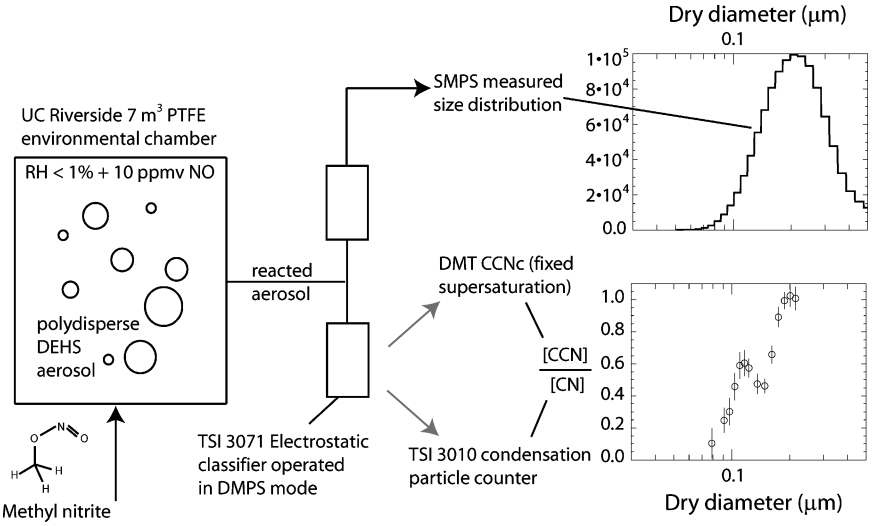

FIG. 1. Schematic of measurement strategy. The two figures on the right show an example size distribution and CCN activation data for a single experiment. Vertical bars in the bottom figure represent ±2 standard deviations, computed from ∼60 independent data points.

a bias in estimation of the critical dry diameter and to nonmonotonic CCNc response when D_c is less than the mode diameter of the polydisperse size distribution. Finally, we use the model to determine the critical diameter of measured activation spectra that were evidently "contaminated" with multiply-charged particles.

2. METHODS

Our experimental setup is illustrated in Figure 1. We performed laboratory experiments measuring the CCN activity of diethylhexyl sebacate (DEHS) reacted with OH inside a ∼7 m^3 PTFE chamber (Lim and Ziemann 2005) that has blacklights for photolysis (λ_{max} ∼ 360 nm). Particles were generated by homogeneous nucleation of heated organic vapor and introduced to the chamber (Docherty and Ziemann 2006). Hydroxyl radicals were generated by photolysis of 10 ppmv of methyl nitrite in the presence of 10 ppmv of NO (Lim and Ziemann 2005). Particle size was monitored continuously with a scanning mobility particle sizer (SMPS). The instrument was operated at 2.5:0.5 sheath-to-monodisperse flow ratio. The scan cycle involved an exponential voltage ramp from low to high (upscan) and high to low (downscan), each taking 120 s. We adjusted the lower and upper voltages to optimize the number of data points. The lower voltage ranged from ∼20–100 V and the upper from ∼1500–6000 V. The resulting electrical mobility spectra were inverted to size distributions, with a charge correction up to +6 charges being applied. An example size distribution of the reacted DEHS aerosol is shown in Figure 1.

Product particles, sampled directly from the environmental chamber, were charge neutralized by passing the aerosol through two ^{210}Po bipolar neutralizers, each containing four two-month-old strips. Charge-equilibration was verified by removing one of the neutralizers. No change in the total concentration and activated fractions was observed, indicating that one neutralizer was sufficient to bring the sample to equilibrium. The charge-equilibrated particles were mobility-selected using a DMA (TSI 3071) and processed in a CCN counter (Droplet Measurement Systems) (Roberts and Nenes 2005), while simultaneously the total particle concentration transmitted to the CCN instrument was measured (TSI 3010). The CCN instrument was operated at 10:1 sheath-to-sample flow rate. The streamwise temperature difference set by the instrument was 5.41, 8.49, 10.57, and 12.66°C. This corresponded to 0.33, 0.53, 0.64, and 0.75% supersaturation, S,determined from CCNc response curves with calibration aerosol. Calibrations were performed with atomized, dried, charge-neutralized, and size-selected ammonium sulfate particles. The measured critical diameter was converted to a critical supersaturation using a single parameter representation of Köhler theory (Petters and Kreidenweis 2007), assuming κ = 0.6. The repeatability in the calibrated critical supersaturations was 2σ = 0.042% (n = 13). The electrostatic classifier (TSI 3071) was operated at 10:2 sheath-to-monodisperse flow ratio and was used to size select particle prior to the CCN measurement. We scanned dry diameter at fixed supersaturation in the CCN instrument. Scans were conducted over the range of S = 0.33% to 0.75%, each scan lasting ∼20 min. For each size, the voltage was set manually and held constant for ∼120 s. During data processing we selected a 60 s subset of these intervals to calculate the ratio of CCN and CN concentration.

Each scan results in a CCNc response curve. An example response curve is shown in Figure 1 (bottom right figure). The response is non-monotonic with three 50% activation diameters. Results and interpretation of the data from this and similar experiments are reported in detail elsewhere (Petters et al. 2006; Prenni et al. 2006). Here we focus on a model that describes the non-monotonic response.

3. THEORY

In this section we develop the activation model. In a first step we review the relevant equations governing the DMA. The DMA classifies particles according to electrical mobility, Z. The mobility centroid, Z^*, of the transfer function for a cylindrical DMA column was first derived by Knutson and Whitby (1975)

$$Z^* = \frac{Q_{sh} + Q_e}{4\pi LV} \ln\left[\frac{R_2}{R_1}\right], \quad [1]$$

where Q_{sh} is the volumetric sheath flow, Q_e is the volumetric excess flow, L is the length of the DMA column, V is the negative potential applied to the inner cylinder, and R_1 and R_2 are the radial location of the aerosol exit and entrance, respectively.

The full-width-half-maximum interval, Δz, of the ideal, non-broadened triangular transfer function was given as

$$\Delta Z = \frac{Q_a + Q_s}{Q_{sh} + Q_e} Z^*, \quad [2]$$

where Q_a is the volumetric aerosol flow rate and Q_s is the volumetric sample flow rate. The transfer function, $\Lambda(Z)$, is a triangular weighting function. At the centroid mobility, $\Lambda(Z^*) = 1$ and at the full-width-half-max, $\Lambda(Z^* - 0.5\Delta Z) = \Lambda(Z^* + 0.5\Delta Z) = 0.5$. No transmission occurs beyond the boundaries of $Z^* \pm \Delta Z$, i.e., $\Lambda(Z^* - \Delta Z) = \Lambda(Z^* + \Delta Z) = 0$.

Deviations from the triangular transfer function may occur due to well-known sources of broadening such as particle diffusion, nonuniform distribution of the particles in the inlet, imperfections in the electrode geometry or imperfections of the flow field (Flagan 1999). The flow ratio of 10:2 used in this study minimizes broadening due to particle diffusion and the relative degradation of $\Lambda(Z)$ due to this source alone, calculated based on Equation (64) of Flagan (1999), is less than ~0.5% for 0.1 μm particles. We therefore consider the triangular transfer model as sufficiently accurate for our application.

With the assumption of unit dynamic shape factor, the sphere equivalent mobility diameter can be calculated from

$$D_{Z,n} = \frac{neC_c(D)}{3\pi\mu Z}, \quad [3]$$

where e is the elementary charge, C_c is the Cunningham slip flow correction factor, μ is the dynamic viscosity of air and n is the number of elementary charges on the particle.

The fraction of particles carrying n charges at charge equilibrium, $f(D, n)$, is calculated according to the Wiedensohler (1988) parameterization

$$\log_{10}[f(D, n = +1, +2)] = \sum_{i=0}^{5} a_i(n)(\log_{10} D)^i, \quad [4]$$

for $n = +1$ and $+2$ and where $a_i(n)$ are fitted coefficients which we obtained from the most recent DMA (TSI 3081) manual and

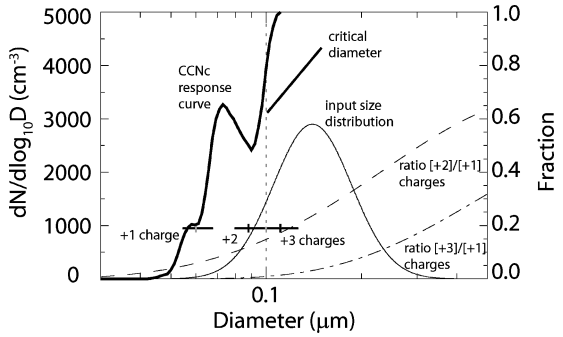

FIG. 2. Calculated CCNc response curve (thick solid line, right ordinate, as function of mobility selected diameter) for log-normally distributed, charge-equilibrated particles transmitted through an ideal DMA followed by transit through an ideal CCN instrument. Shown are an assumed log-normal input size distribution (solid line, left ordinate, $N = 900$ cm^{-3}, $D_g = 0.14$ μm, $s_g = 1.33$), the ratio of [+2]/[+1] (dashed line) and [+3]/[+1] (dashed-dotted line) charges at charge equilibrium (right ordinate), the assumed critical diameter for the model calculations (dotted line), the centroid sphere equivalent mobility diameter, and the mobility band-width for +1, +2, and +3 (from left to right) charged particles transmitted through the TSI long DMA column at an assumed 10:2 sheath-to-monodisperse flow ratio (gray intervals).

for $n = +3$,

$$\ln[f(D, n = +3)] = \ln\left[\frac{e}{\sqrt{4\pi^2\varepsilon_0 DkT}}\right] - \frac{\left(n - \frac{2\pi\varepsilon_0 DkT}{e^2}\ln[r]\right)^2}{\frac{4\pi\varepsilon_0 DkT}{e^2}}, \quad [5]$$

where k is Boltzmann's constant, ε_0 is the dielectric constant and $r = 0.875$ is the ion mobility ratio. The variation of $f(D, n = +2)/f(D, n = +1)$ and $f(D, n = +3)/f(D, n = +1)$ with the mobility diameter is shown in Figure 2 by the dashed and dashed-dotted lines, respectively. For $D < 0.1$ μm, the ratio of doubly-charged to singly-charged particles of a given size is less than 20%. The fraction of triply-charged particles is negligible. For $D = 0.3$ μm, however, the combined fraction of doubly- and triply-charged particles exceeds 60% when ratioed to the singly charged concentration. Also shown in Figure 2 are the centroid (vertical gray bars) and width of the transfer function (horizontal gray bars) for $n = +1$, $+2$, and $+3$ (left to right) particles at one selected potential, $V = 623$V, $Q_a = Q_s = 2$ lpm and $Q_{sh} = Q_e = 10$ lpm.

Shown are an assumed log-normal input size distribution (solid line, left ordinate, $N = 900$ cm^{-3}, $D_g = 0.14$ μm, $\sigma_g = 1.33$), the ratio of [+2]/[+1] (dashed line) and [+3]/[+1] (dashed-dotted line) charges at charge equilibrium (right ordinate), the assumed critical diameter for the model calculations (dotted line), the centroid sphere equivalent mobility diameter, and the mobility band-width for +1, +2, and +3 (from left to right) charged particles transmitted through the TSI long DMA column at an assumed 10:2 sheath-to-monodisperse flow ratio (gray intervals).

A log normal size distribution with $N = 900$ cm^{-3}, $D_g = 0.14$ μm, and $\sigma_g = 1.33$. is assumed for the representative

calculations shown in Figure 2. For the determination of the CCNc response, the input size distribution, dN/dD, must be transformed into the mobility domain. Application of the chain rule gives:

$$\frac{dN_n}{dZ} = \frac{dD}{dZ}\frac{dN}{dD}, \quad [6]$$

where dN_n/dZ is the differential size distribution of +n-charged particles in the mobility domain, and the derivative dD/dZ is given by differentiation of Equation (3). Because the slip correction factor is not constant, numerical differentiation is convenient. In Figure 2 we indicate the assumed critical diameter ($D_c = 0.1\ \mu$m) with the vertical dotted line.

We now can calculate an idealized CCN instrument response to varying the mobility centroid for the assumed input size distribution. The number concentration of particles transmitted to the CCN instrument, N_{CN}, is determined as follows: for an array of electrical mobility we (1) determine the mobility diameter of the particles carrying +1 charge, (2) determine the fraction of total particles that they represent according to charge equilibrium, (3) weigh the result by the triangular transfer function of the DMA, (4) weigh the result by the particle size distribution, and (5) integrate the result over the mobility bandwidth, $Z^* \pm \Delta Z$. Steps 1–5 give the contribution of the singly-charged particles. Repeating steps 1–5 for +2 and +3 charged particles and summing the results gives the total number of particles transmitted through the DMA. Mathematically,

$$N_{CN}(D_{Z^*}) = \sum_{n=1}^{3}\left[\int_{Z=Z^*+\Delta Z}^{Z=Z^*-\Delta Z} f(D_{Z,n}, n)\Lambda(Z)\frac{dN_n}{dZ}dZ\right]. \quad [7]$$

Note that a centroid mobility Z^* must be assumed to define $\Lambda(Z)$ and the mobility centroid Z^* is interpreted as the mobility diameter of +1 charged particles ($D_{Z^*,1}$). Since the diameters used in this study are much larger than the minimum detected size by the CPC ($\sim$0.015 μm), the CPC counting efficiency does not depend on the number of charges carried by the particle, and the detector efficiency can be assumed equal to unity, the term was omitted in Equation (7).

Using the same arguments we can also calculate the number of particles that activate as CCN:

$$N_{CCN}(D_{Z^*}) = \sum_{n=1}^{3}\left[\int_{Z=Z^*+\Delta Z}^{Z=Z^*-\Delta Z} g(D_{Z,n})f(D_{Z,n}, n)\Lambda(Z)\frac{dN_n}{dZ}dZ\right], \quad [8]$$

where $g(D_{z,n})$ is a function that gives the fraction of particles that activate as cloud droplets. For an ideal CCN instrument all particles larger than D_c will activate into cloud droplets and particles smaller than D_c will not. Thus $g(D \geq D_c) = 1$ and $g(D < D_c) = 0$.

For some CCN instruments broadening of the activation spectrum has been observed (Snider et al. 2006), and for these instruments $g(D_{z,n})$ must take a different form. However, this form remains uncharacterized to date.

The activated fraction is calculated from Equations (7) and (8)

$$A(D_{Z^*}) = \frac{N_{CCN}(D_{Z^*})}{N_{CN}(D_{Z^*})}. \quad [9]$$

The computed activated fraction as a function of mobility diameter is shown in Figure 2. For this hypothetical example $D_c = 0.1\ \mu$m and the critical diameter lies on the ascending branch of a relatively narrow size distribution. The activation curve exhibits a shoulder at $D \sim 0.06\ \mu$m, a local maximum at $D \sim 0.073\ \mu$m, and a local minimum at $D \sim 0.089\ \mu$m. There are three mobility diameters for which the activated fraction equals 50%. None of the calculated D_{50}s corresponds to the actual critical diameter. Smoothing through the response curve would also yield a calculated D_{50} that is less than the critical diameter.

The calculated CCNc response curve suggests that the total quasi-monodisperse particle number concentration is dominated by multiply-charged particles. For the example CCNc response curve shown in Figure 2, and an assumed potential of 623 V, the centroid mobility diameters of singly-, doubly-, and triply-charged particles are $D_{Z^*,1} = 0.06\ \mu$m, $D_{Z^*,2} = 0.087\ \mu$m, and $D_{Z*,3} = 0.11\ \mu$m (gray bars). Their relative contribution, expressed as number concentration ratio is $N_{Z*,1}$:$N_{Z*,2}$:$N_{Z*,3}$ = 22:60:18. The triply-charged particles exceed the critical diameter ($D_c = 0.1\ \mu$m) and are activated as CCN in the model. This explains the activated fraction of 0.18 at $D_{Z^*,1} = 0.06\ \mu$m. The steep increase between $0.06 < D < 0.073\ \mu$m, where the local maximum occurs, is due to activation of doubly-charged particles. At the local maximum, $D_{Z^*,1} = 0.073\ \mu$m: $D_{Z*,2} = 0.108\ \mu$m: $D_{Z^*,3} = 0.138\ \mu$m and $N_{Z^*,1}$:$N_{Z^*,2}$:$N_{Z^*,3}$ = 35:51:14. For $D \geq 0.073\ \mu$m, all doubly-charged particles exceed the assumed critical diameter of 0.1 μm. Further increases in the mobility diameter lead to an increase in the singly-charged:multiply-charged ratio. But the singly-charged particles are still too small to activate, caused by a gap between the $D_{Z^*,1}$ and $D_{Z^*,2}$ transfer functions, leading to a decrease in the CCNc response curve. At the local minimum ($D_{Z^*,1} = 0.089\ \mu$m: $D_{Z^*,2} = 0.133\ \mu$m: $D_{Z^*,3} = 0.171\ \mu$m, $N_{Z^*,1}$:$N_{Z^*,2}$:$N_{Z^*,3}$ = 52:40:8), the right tail of the transfer function for the singly-charged particles now equals the critical diameter. Finally, at the critical diameter (dotted line), $\sim$80% of the total population are activated. However, doubly and triply-charged particles represent 36% of the selected particles.

From this example it is possible to draw some general conclusions about the interference of multiply-charged particles on the interpretation of CCNc data. When sampling from the ascending branch of the size distribution, and when the geometric standard deviation is small ($\sigma_g < 1.5$), the concentration ratio $N_{Z^*,1}$:$N_{Z^*,2}$:$N_{Z^*,3}$ is skewed strongly toward multiply charged particles, thereby increasing their contribution to the activated

fraction. The equilibrium fraction of multiply-charged particles increases with size. Thus, size distributions with large mode diameters are more likely to exhibit this artifact in CCNc response.

4. INVERSION

The calculated CCNc response curves, defined by Equations (1)–(9), can be used to determine the critical diameter from experimental data. Calculating $A(D_{Z^*})$ requires knowledge of the DMA geometry (L, R_1, R_2), the sheath and aerosol flow rates (Q_{sh}, Q_a), the applied negative potential (V), the polydisperse size distribution (e.g., N, D_g, σ_g, or a data histogram) and D_c. When size distribution data are available, $A(D_{Z^*})$ may be calculated for an assumed value of D_c. The χ^2-statistic for an assumed D_c is

$$\chi^2(D_c) = \sum_i \frac{\left(A_{observed}(D_{Z_i^*}) - A_{calculated}(D_{Z_i^*})\right)^2}{A_{calculated}(D_{Z_i^*})}. \quad [10]$$

Minimizing the χ^2-statistic by varying the assumed D_c gives best the estimate of the critical diameter of the sample. We demonstrate this procedure using measured activation data from one experiment.

Figure 3 shows activation data, $A_{observed}(D_{Z^*})$ (circles), for the DEHS+OH aerosol sampled at a single supersaturation (Figures 3a, b). In Figure 3a, the histogram is the SMPS particle size distribution measured in the middle of the sampling period. It was used in our calculations of $A_{calculated}(D_{Z^*})$ for the assumed values of $D_c = 0.1$ and 0.3 μm, indicated by the left and right dashed lines, respectively in Figure 3a. For these two values there is poor agreement between the calculated and measured CCNc response curves. This is reflected in the poor χ^2-statistic shown in Figure 3c. There we show the variation of the χ^2-statistic as a function of the scanned critical diameter, where we have normalized the χ^2-curve by the maximum value in the assumed D_c domain ($0.1 < D_c < 0.23$ μm). The curve shows a pronounced minimum at $D_c = 0.19$ μm, which we have indicated with the vertical dotted line in Figures 3a,c. The corresponding CCNc response curve is shown by the solid line in Figure 3a, and is in good qualitative agreement with the measured values. It captures both the diameter and magnitude of the doublet-peak to the left of the critical diameter. We also calculated the Pearson correlation coefficient (R) between the calculated and observed CCNc response and, for this example, $R^2 = 0.97$.

The inversion procedure fails in the absence of accurate size distribution data. We show this in Figure 3b. There we plot the same activation data, but we have artificially biased the input size distribution by shifting the mode diameter ~0.1 μm toward smaller sizes. We repeated the steps that went into the construction of Figures 3a and 3c with this artificially biased size spectrum. Although the minimum in the χ^2-curve persists, the shape of the CCNc response curves is markedly different. Most notably, the magnitude of the doublet peak changed for the same assumed critical diameters when compared to Figures 3a ($D_c = 0.1$ and 0.3 μm, dashed lines). The χ^2-value at the minimum (Figure 3d) is greater than in the unbiased case (Figure 3c). Furthermore, the agreement with the measured and calculated CCNc response curve is poor ($R^2 = 0.42$) even at the minimum of the χ^2-curve. Most importantly, the inferred critical diameter is smaller than in the unbiased case ($D_c = 0.13$ μm).

Figure 4 shows activation data, $A_{observed}(D_{Z^*})$ (circles), from the DEHS+OH experiment, sampled at four chamber

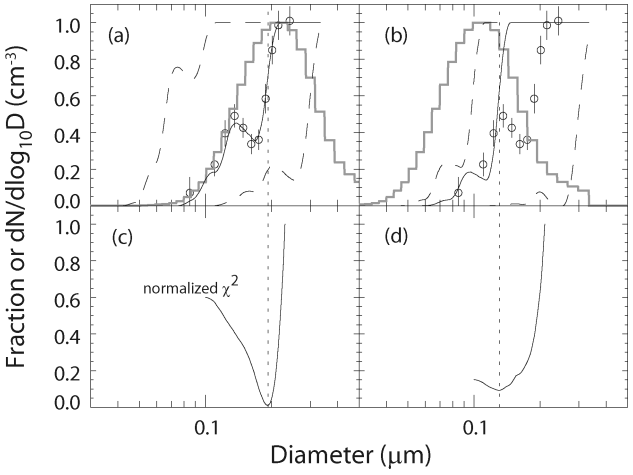

FIG. 3. Panels (a, b): Measured CCNc response (circles) for DEHS+OH experiment at $S = 0.64\%$. Vertical bars represent ±2 standard deviations, computed from ~60 independent data points. Gray histogram, panel a: normalized spectral density of the input size distribution. Gray histogram, panel b: same as figure a, but the mode diameter is shifted by ~0.1 μm toward smaller sizes. Dashed and solid lines, panels a, b: Calculated CCNc response curves for various assumed D_c (see text). Panels c, d: Normalized χ^2-statistic as a function of assumed values of D_c. The minimum value (dotted line) is used to determine the best-fit CCNc response curve.

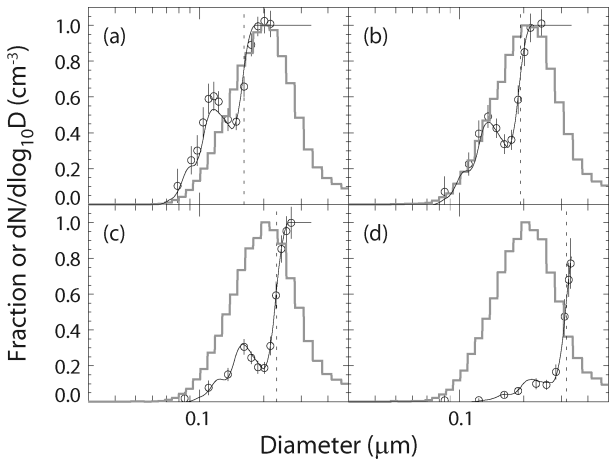

FIG. 4. Measured CCNc response (circles) for DEHS+OH experiment; (a) $S = 0.75\%$, (b) $S = 0.64\%$, (c) $S = 0.53\%$, (d) $S = 0.33\%$. Vertical bars represent ±2 standard deviations, computed from ~60 independent data points. Gray histogram: normalized spectral density of the input size distribution. Solid line: best-fit CCNc response curve. The critical diameter yielding the best fit to the observation is indicated by the dotted line; (a) $D_c = 0.16$ μm, (b) $D_c = 0.19$ μm, (c) $D_c = 0.23$ μm, (d) $D_c = 0.32$ μm.

supersaturations (Figures 4a–d). Vertical bars are ±2 standard deviations calculated from ∼60 s of 1 Hz data. Each panel corresponds to a ∼20 min sampling period. The histogram is the SMPS particle size distribution measured in the middle of each sampling period. We used the procedure described above to determine the best-fit critical diameter, indicated by the vertical dotted lines in the figures. The critical diameter is smallest for the largest supersaturation (Figure 4a) and increases with decreasing supersaturation (Figures 4b–4d). In Figure 4a the critical diameter is along the ascending branch of the size distribution and hence the contribution of multiply-charged particles is largest. Their contribution is seen to decrease with increasing critical diameter in both measured and calculated activation curves. For all four supersaturations, $R^2 > 0.96$, indicating that data and model are in good agreement. Notably, the decrease of the magnitude of the multiply-charged particles with increasing critical diameter is captured well by the calculated CCNc response curves.

5. DISCUSSION AND CONCLUSIONS

In contrast to the data presented here, multiply-charged particles appear to less affect calibrations with test aerosol (Hudson 1989; Roberts and Nenes 2005; Snider et al. 2006). However, calibrations are usually performed with hygroscopic solutes whose critical diameters are much less than 0.1 μm and thus multiply-charging effects are less pronounced.

There are two reasons: first, ammonium sulfate test particles are more hygroscopic and for supersaturations >0.3%, critical diameters are smaller than 0.1 μm. Second, and more importantly, dried size distributions generated by commercially available atomizers (e.g. TSI 3076) peak at $0.03 < D_{dry} < 0.08$ μm, depending on the solute concentration, thereby limiting the contribution of multiply-charged particles, which are more prominent at larger mobility diameters. The problem arises when sampling particles with $D_c > 0.1$ μm from particle size distributions with mode diameters also larger than D_c, which often occurs for aerosol that is generated via homogeneous nucleation from the gas phase. This generation method is sometimes preferred when studying pure and chemically-aged organics (Kumar et al. 2003; Broekhuizen et al. 2004a, b; Petters et al. 2006) and is necessary when studying hygroscopic properties of secondary organic aerosol (Huff-Hartz et al. 2005; VanReken et al. 2005). The resulting size distributions are narrow, mode diameters typically exceed 0.1 μm, and the hygroscopicity of the particle is less than that of most atmospherically relevant inorganic compounds, leading to larger activation diameters. In some cases, when thermal gradient diffusion chambers were used, the multiply-charged particles may have gone unnoticed because the activation curves may be instrumentally broadened by as much as a factor of two (Snider et al. 2006). It is likely, then, that the local maximum and minimum visible in the data in Figure 3 are smeared beyond recognition when sampled by an instrument for which broadening is a measurement issue. If this is the case, the observed 50% activation diameter will be smaller than the actual critical diameter, biasing the reported D_c's.

TABLE 1
Comparison between critical diameters inferred from the inversion and those inferred from a sigmoidal fit (Snider et al. 2006)

	Critical Diameter (μm)	
Supersaturation (%)	Inversion	Sigmoidal fit
0.75	0.162	0.121
0.64	0.192	0.160
0.53	0.230	0.217
0.33	0.317	0.311

We fitted the activation data in Figure 4 to a standard sigmoidal model (Snider et al. 2006) and compare the critical diameters to those from the inversion in Table 1. In the worst case, the sigmoidal fit inferred critical diameter is biased low by 41 nm. This bias diminishes with the magnitude of the multiply charged particle peak. The lowest bias, 6 nm, occurs at the lowest supersaturation.

A different method for charge correcting the CCNc response function was suggested by Frank et al. (2006). We compared our inferred critical dry diameters to those predicted by the Frank et al. (2006) model and obtained very similar results.

Doubly-charged particles may also contribute when sampling ambient particles. Although the method described here may be applied to fit ambient data, it is only strictly applicable if the particles are internally mixed and the chemical composition does not vary with particle size. These assumptions are often violated in ambient aerosols, especially close to sources. Additional techniques need to be developed to invert the CCNc response function for this case. One possible approach would be to apply standard inversion procedures developed to obtain size distributions from differential mobility analyzer measurements (Alofs and Balakumar 1982). This technique can be applied independently to the DMA-CPC and DMA-CCN data sets to obtain charge corrected distributions. The ratio of these charge corrected distributions retrieves $g(D_{z,n})$, which was represented as an idealized step function in this study. The value where $g(D_{z,n})$ equals 0.5 corresponds to the critical dry diameter obtained by the method described here. The advantage of using a standard inversion is that no assumptions of the size-dependence of composition or mixing state are required. One disadvantage is that the size range covered with the DMA must be extended to cover the larger particles that may be multiply charged. Additionally, noise in the size and CCN distributions may complicate identification of the critical diameter more so than with the approach described here.

REFERENCES

Alofs, D. J. and Balakumar, P. (1982). Inversion to Obtain Aerosol Size Distributions from Measurements with a Differential Mobility Analyzer, *J. Aerosol Sci.* 13(6):513–527.

Bilde, M. and Svenningsson, B. (2004). CCN Activation of Slightly Soluble Organics: The Importance of Small Amounts of Inorganic Salt and Particle Phase, *Tellus B*, 56(2):128–134.

Broekhuizen, K., Kumar, P. P., and Abbatt, J. P. D. (2004A). Partially Soluble Organics as Cloud Condensation Nuclei: Role of Trace Soluble and Surface Active Species, *Geophys. Res. Lett.* 31(1):L01107.

Broekhuizen, K. E., Thornberry, T., Kumar, P. P., and Abbatt, J. P. D. (2004b). Formation of Cloud Condensation Nuclei by Oxidative Processing: Unsaturated Fatty Acids, *J. Geophys. Res.* 109(D24):D24206.

Corrigan, C. E. and Novakov, T. (1999). Cloud Condensation Nucleus Activity of Organic Compounds: A Laboratory Study, *Atmos. Environ.* 33(17):2661–2668.

Cruz, C. N. and Pandis, S. N. (1997). A Study of the Ability of Pure Secondary Organic Aerosol to Act as Cloud Condensation Nuclei, *Atmos. Environ.* 31(15):2205–2214.

Dinar, E., Taraniuk, I., Graber, E. R., Katsman, S., Moise, T., Anttila, T., Mentel, T. F., and Rudich, Y. (2006). Cloud Condensation Nuclei Properties of Model and Atmospheric HULIS, *Atmos. Chem. Phys.* 6:2465–2481.

Docherty, K. S. and Ziemann, P. J. (2006). Reaction of Oleic Acid Particles with NO_3 Radicals: Products, Mechanism, and Implications for Radical–Initiated Organic Aerosol Oxidation, *J. Phys. Chem. A.* 110:3567–3577.

Flagan, R. C. (1999). On Differential Mobility Analyzer Resolution, *Aerosol Sci. Technol.* 30(6):556–570.

Frank, G. P., Dusek, U., and Andreae, M. O. (2006). Technical Note: A Method for Comparing Size–Resolved CCN in the Atmosphere, *Atmos. Chem. Phys. Discuss.* 6:4879–4895.

Hudson, J. G. (1989). An Instantaneous CCN Spectrometer, *J. Atmos. Ocean. Technol.* 6(6):1055–1065.

Huff–Hartz, K. E. H., Rosenorn, T., Ferchak, S. R., Raymond, T. M., Bilde, M., Donahue, N. M., and Pandis, S. N. (2005). Cloud Condensation Nuclei Activation of Monoterpene and Sesquiterpene Secondary Organic Aerosol, *J. Geophys. Res.* 110(D14):D14208.

Knutson, E. O. and Whitby, T. B. (1975). Aerosol Classification by Electric Mobility: Apparatus, Theory, and Applications, *J. Aerosol Sci.* 6:443–451.

Kumar, P. P., Broekhuizen, K., and Abbatt, J. P. D. (2003). Organic Acids as Cloud Condensation Nuclei: Laboratory Studies of Highly Soluble and Insoluble Species, *Atmos. Chem. Phys.* 3:509–520.

Lim, Y. B. and Ziemann, P. J. (2005). Products and Mechanism of Secondary Organic Aerosol Formation from Reactions of n–Alkanes with OH Radicals in the Presence of NOx, *Environ. Sci. Technol.* 39(23):9229–9236.

Petters, M. D. and Kreidenweis, S. M. (2007). A Single Parameter Representation of Aerosol Hygroscopicity and Cloud Condensation Nucleus Activity, *Atmos. Chem. Phys.* 7:1961–1971.

Petters, M. D., Prenni, A. J., Kreidenweis, S. M., DeMott, P. J., Matsunaga, A., Lim, Y. B., and Ziemann, P. J. (2006). Chemical Aging and the Hydrophobic–to–Hydrophilic Conversion of Carbonaceous Aerosol, *Geophys. Res. Lett.* submitted.

Prenni, A. J., DeMott, P. J., Kreidenweis, S. M., Sherman, D. E., Russell, L. M., and Ming, Y. (2001). The Effects of Low Molecular Weight Dicarboxylic Acids on Cloud Formation, *J. Phys. Chem. A.* 105(50):11240–11248.

Prenni, A. J., Petters, M. D., DeMott, P. J., Kreidenweis, S. M., Ziemann, P. J., Matsunaga, A., and Lim, Y. B. (2006). Cloud Drop Activation of Secondary Organic Aerosol, *J. Geophys. Res.* submitted.

Roberts, G. C. and Nenes, A. (2005). A Continuous-Flow Streamwise Thermal-Gradient CCN Chamber for Atmospheric Measurements, *Aerosol Sci. Technol.* 39(3):206–221.

Shantz, N. C., Leaitch, W. R., and Caffrey, P. F. (2003). Effect of Organics of Low Solubility on the Growth Rate of Cloud Droplets, *J. Geophys. Res.* 108(D5):4168.

Snider, J. R., Petters, M. D., Wechsler, P., and Liu, P. S. K. (2006). Supersaturation in the Wyoming CCN Instrument, *J. Atmos. Ocean. Technol.* 23(10):1323–1339.

VanReken, T. M., Ng, N. L., Flagan, R. C., and Seinfeld, J. H. (2005). Cloud Condensation Nucleus Activation Properties of Biogenic Secondary Organic Aerosol, *J. Geophys. Res.* 110(D7):D07206.

Wiedensohler, A. (1988). An Approximation of the Bipolar Charge-Distribution for Particles in the Sub-Micron Size Range, *J. Aerosol Sci.* 19(3):387–389.